Geophysical Research Letters

RESEARCH LETTER
10.1029/2025GL116191

Diminished Chandler Wobble After 2015: Link to Mass Anomalies in 2011

Taehwan Jeon[1], Ki-Weon Seo[2], Kookhyoun Youm[2], Jooyoung Eom[3], Daeha Lee[2], Jianli Chen[4,5,6], and Clark R. Wilson[7,8]

[1]Center for Educational Research, Seoul National University, Seoul, Republic of Korea, [2]Department of Earth Science Education, Seoul National University, Seoul, Republic of Korea, [3]Department of Earth Science Education, Kyungpook National University, Daegu, Republic of Korea, [4]Department of Land Surveying and Geo-Informatics, The Hong Kong Polytechnic University, Hong Kong, China, [5]Research Institute for Land and Space, The Hong Kong Polytechnic University, Hong Kong, China, [6]The Hong Kong Polytechnic University Shenzhen Research Institute, Shenzhen, China, [7]Center for Space Research, University of Texas at Austin, Austin, TX, USA, [8]Department of Earth and Planetary Sciences, Jackson School of Geosciences, University of Texas at Austin, Austin, TX, USA

Abstract Observed polar motion after 2015 is dominated by the annual wobble, due to unprecedented amplitude reduction of the Chandler Wobble component. This change is likely due to suppression of the 433-day-period free wobble by geophysical excitation sources. Our experiments show that excitation changes in the period 2011–2012 are the most significant contributors to the diminished Chandler Wobble after 2015. Numerical models and satellite observations suggest that the Chandler Wobble suppression was largely driven by the 2011–2012 changes in continental-scale air and terrestrial water mass redistribution.

Plain Language Summary The Chandler Wobble is a free oscillation of the Earth's rotation pole with a period of about 433 days. Various geophysical processes contribute to maintaining this wobble, and may also attenuate the motion. The amplitude of Chandler Wobble greatly diminished after 2015, and this unprecedented event suggests an attenuation cause by large scale geophysical phenomena. We analyzed the time-dependent frequency patterns of polar motion excitation using the wavelet transform, and found excitation in 2011–2012 to be the dominant cause of the subsequent Chandler Wobble amplitude reduction. Geophysical models of excitation sources showed a similar time-dependent frequency pattern, and the 2011–2012 excitation changes were closely associated with the air and water mass anomalies, after the 2010–2011 La Niña event.

Key Points:

- Polar motion excitation in 2011–2012 is the strongest contributors to diminished Chandler Wobble amplitude after 2015
- Polar motion excitation anomalies in this period are closely associated with air and terrestrial water storage changes

Supporting Information:

Supporting Information may be found in the online version of this article.

Correspondence to:

K.-W. Seo,
seokiweon@snu.ac.kr

Citation:

Jeon, T., Seo, K.-W., Youm, K., Eom, J., Lee, D., Chen, J., & Wilson, C. R. (2025). Diminished Chandler Wobble after 2015: Link to mass anomalies in 2011. *Geophysical Research Letters*, *52*, e2025GL116191. https://doi.org/10.1029/2025GL116191

Received 26 MAR 2025
Accepted 8 SEP 2025

Author Contributions:

Conceptualization: Taehwan Jeon, Ki-Weon Seo, Clark R. Wilson
Data curation: Taehwan Jeon, Kookhyoun Youm
Investigation: Taehwan Jeon, Kookhyoun Youm, Jooyoung Eom, Daeha Lee
Methodology: Taehwan Jeon, Ki-Weon Seo, Kookhyoun Youm, Jooyoung Eom, Daeha Lee, Jianli Chen, Clark R. Wilson
Resources: Jooyoung Eom
Supervision: Ki-Weon Seo
Validation: Taehwan Jeon, Ki-Weon Seo
Visualization: Taehwan Jeon
Writing – original draft: Taehwan Jeon, Ki-Weon Seo, Jianli Chen, Clark R. Wilson

1. Introduction

The Chandler Wobble (CW) is a free mode of the Earth, producing movement of the rotational pole relative to a body-fixed reference frame. The circular motion of the rotational pole near geographical north pole has an amplitude typically near 10 m in diameter, with a period near 433 days or about 0.8435 cycles per year (cpy), a frequency controlled by the Earth's shape and physical properties (Gross, 2000; Munk & MacDonald, 1960). The proximity of the Chandler frequency, f_c, to the annual frequency leads to resonant amplification of annual excitation sources, causing also an additional annual wobble. Because damping would cause the CW to decay to zero in the absence of excitation sources, its persistence since the earliest observations in the 1840s shows, on average, a balance between damping and excitation sources, such as winds, ocean currents, and mass redistribution of water, ice, air, and the solid Earth (Bizouard et al., 2011; Chao & Chung, 2012; Gross, 2000; Malkin & Miller, 2010). However, there have been anomalous intervals, the first recognized being 1925–1940, when the CW amplitude diminished significantly, with an associated large phase shift (Fedorov & Yatskiv, 1965; Guinot, 1972; Malkin & Miller, 2010; Vondrak & Ron, 2005). Using numerical experiments, Chao and Chung (2012) showed that this was likely due to random excitation variations, which are able to cause a decline in CW amplitude as well as, at most times, maintaining it in the presence of damping.

A second CW amplitude reduction event has been observed during the last decade (Yamaguchi & Furuya, 2024), and is the focus of this study. This event is likely associated with cancellation from excitation sources, as proposed for the 1925–1940 event. However, the recent event should be suited to more detailed study, given improved data quality and estimates of excitation sources that have become available. Recently, Xu et al. (2024) examined reduction in CW amplitude due to cancellation related to the atmosphere and oceans. Although these are the dominant excitation sources (Gross, 2000), there are also important contributions from terrestrial water storage

Writing – review & editing:
Taehwan Jeon, Ki-Weon Seo, Jianli Chen, Clark R. Wilson

changes, and there is some uncertainty as to the CW quality factor (Q_c) that may affect the analysis. Yamaguchi and Furuya (2024) found that it was not easy to reproduce the CW amplitude reduction event using currently available excitation estimates, because Earth's resonance at the Chandler frequency causes a small change in the excitation model to result in larger differences in predicted CW amplitude.

In this study, we develop a separation of the CW motion into a free wobble (that would persist without further excitation) and a forced wobble due to excitation sources. The amplitude reduction results from cancellation between free and forced wobbles (Munk & MacDonald, 1960) when the forced wobble is out-of-phase with respect to the free wobble. We find the reduction after 2015 related to excitation sources as early as 2011, as seen in both geodetic excitation computed from polar motion observations, and geophysical models-derived excitation of air and terrestrial water.

2. Materials and Methods

2.1. CW Time Series and Excitation Function From Geodetic Polar Motion Observation

We used the latest version of the Earth Orientation Parameters (EOP), EOP 20 C04 IAU2000A data, distributed by the International Earth Rotation and Reference Service (IERS), which is very similar to the EOP 14 C04 products (Bizouard et al., 2019). EOP 20 C04 provides observed polar motion from 1962 to the present, and the data from 1980.0 to 2024.0 is used to investigate the CW amplitude reduction event after ~2015. Here we used the monthly solutions for subsequent comparison with the estimates from monthly excitation functions (e.g., estimates from Satellite Laser Ranging), as described below. The polar motion components m_1 and m_2 (gray curves in Figures 1a and 1b) represent the x- and y-directional displacements of the pole position, positive toward the Greenwich meridian and 90° East longitude, respectively.

The excitation function at time t can be obtained from observed polar motion via a linearized Liouville equation (Munk & MacDonald, 1960) such as

$$\mathbf{\Psi}(t) = \frac{i}{\sigma_c}\frac{d\mathbf{m}(t)}{dt} + \mathbf{m}(t) \tag{1}$$

where Ψ and $\mathbf{m}$ are the complex forms of excitation and polar motion, such as $\psi_1 + i\psi_2$ and $m_1 + im_2$, respectively. Here, σ_c represents a complex angular frequency including the Chandler frequency f_c and the damping factor Q_c, such as

$$\sigma_c = 2\pi f_c\left(1 + \frac{i}{2Q_c}\right) \tag{2}$$

where $f_c = 1/P_c$. There are diverse estimates for P_c and Q_c in previous studies (Ding & Chao, 2017; Furuya & Chao, 1996; Gross, 2005; Nastula & Gross, 2015; Seitz et al., 2012; Wilson & Vicente, 1990; Xu et al., 2024). In the literature, the CW period ranges from ~430 to ~434 days, and Q_c has more extensive range, from ~40 to ~180. We considered $P_c = 433$ days, and $Q_c = 100$ in this paper, but also discuss results using different P_c and Q_c values below.

Equation 1 can be solved in the discrete form (Wilson, 1985) such as

$$\mathbf{\Psi}_t = \frac{i}{\sigma_c}\frac{1}{2\Delta t}e^{-i\pi f_c \Delta t}\left[-e^{i\sigma_c \Delta t}\mathbf{m}_{t-\Delta t} + \left(1 - e^{i\sigma_c \Delta t}\right)\mathbf{m}_t + \mathbf{m}_{t+\Delta t}\right] \tag{3}$$

where Ψ_t and $\mathbf{m}_t$ indicate the discrete samples of the continuous functions of $\Psi(t)$ and $\mathbf{m}(t)$ at time t, respectively, and Δt represents the sampling interval. The computed Ψ changes are shown as Figures 1c and 1d (red curves).

The solution of Equation 1 for $\mathbf{m}$ is (Munk & MacDonald, 1960)

$$\mathbf{m}(t) = \mathbf{m}_0 e^{i\sigma_c t} - i\sigma_c \int_0^t \mathbf{\Psi}(\tau)\, e^{i\sigma_c (t-\tau)}\, d\tau. \tag{4}$$

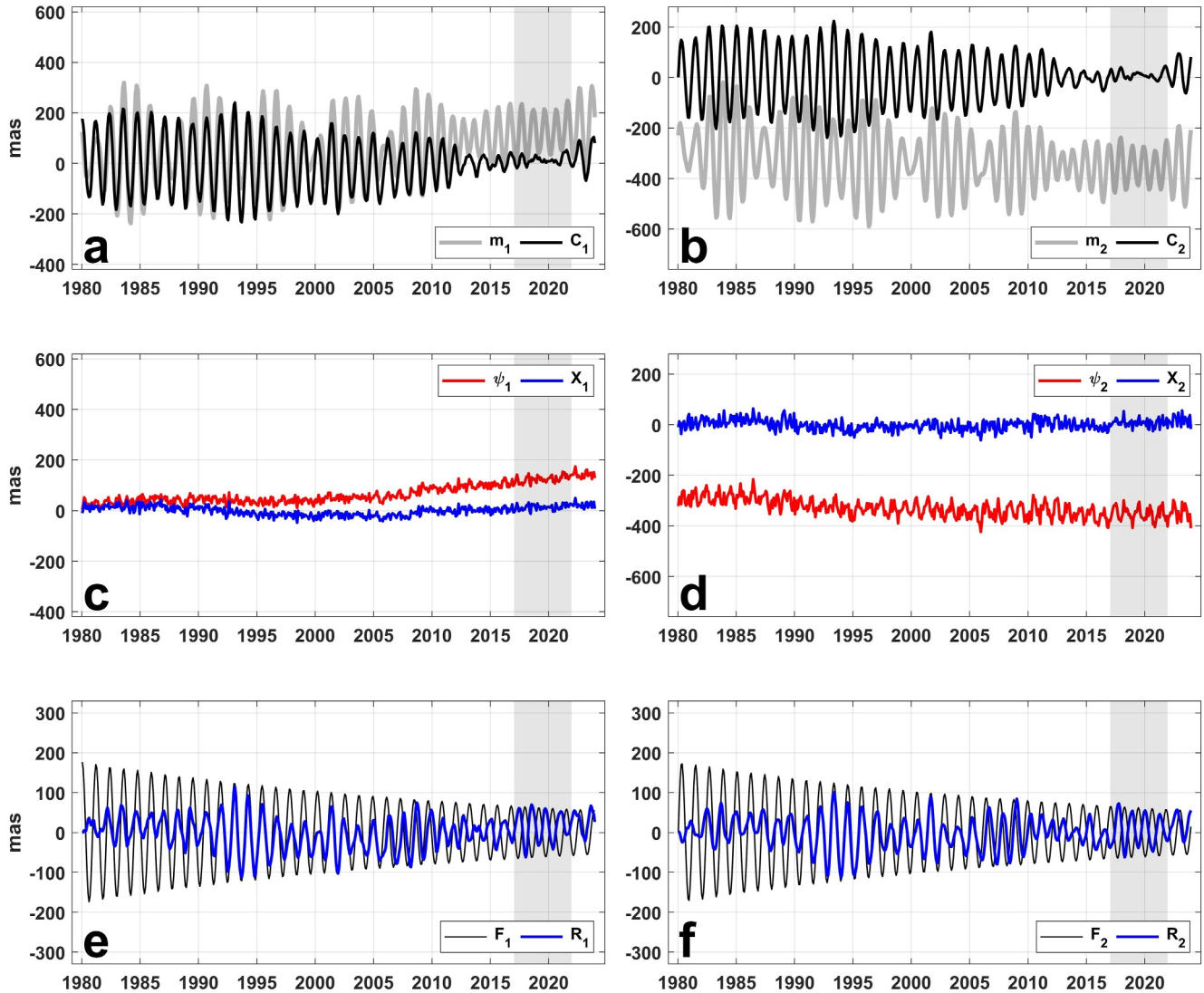

Figure 1. Chandler Wobble (CW) time series from polar motion observation and its decomposition. (a, b) *x*- and *y*-directional changes of polar motion (**m**, gray) and the CW time series (**C**, black) from International Earth Rotation and Reference Service Earth Orientation Parameters C04. (c, d) Excitation functions from the full polar motion observation (Ψ, red), and those from the CW time series (**X**, blue). **X** is also obtained when removing annual variations and linear component from Ψ. (e, f) The free (**F**, black) and forced wobble (**R**, blue) from decomposing **C**. Note that **F** is the 433-day oscillation due to the first value of **C** in panels (a, b), and **R** is accumulated effect of **X** in panels (c, d). The gray shaded area represents 2017.0–2022.0 period when the observed **C** amplitude is minimal.

$\mathbf{m}_0$ represents the initial value (at $t = 0$) of the polar motion, and we set 1980.0 as $t = 0$ for the computations shown in Figure 1. The first term of the right hand side of Equation 4 represents the free wobble due to the initial condition of polar motion, and the second term indicates the forced wobble due to the accumulated effect of the excitation function Ψ. By definition, the first value of the forced wobble (at $t = 0$) is 0.

The CW time series (denoted here as $\mathbf{C} = C_1 + iC_2$) are often examined by removing the annual variation and the linear component from **m** (e.g., Chao & Chung, 2012, Yamaguchi & Furuya, 2024), such as the black curves in Figures 1a and 1b. This reduction for **m** changes both contributions of the free and forced wobbles in Equation 4. For example, the excitation function Ψ reduces to **X**, which is free of trend, bias, and annual changes (blue curves in Figures 1c and 1d), and $\mathbf{m}_0$ also changes to $\mathbf{C}_0$ due to the first values of the removed contributions. Obviously, $\mathbf{C}_0$ is equivalent to the first value of the time series of **C**. Consequently, the change of **C** can be expressed in a similar form via Equation 4,

$$\mathbf{C}(t) = \mathbf{F}(t) + \mathbf{R}(t) = \mathbf{C}_0 e^{i\sigma_c t} - i\sigma_c \int_0^t \mathbf{X}(\tau)\, e^{i\sigma_c (t-\tau)}\, d\tau \tag{5}$$

where **F** and **R** indicate the first term (free wobble) and the second term (forced wobble) of the right hand side of Equation 5, respectively. The forced wobble contribution **R** can be computed by removing **F** from **C** or by integrating effect due to **X**. The latter can be solved via the discrete polar motion equation (Wilson, 1985):

$$\mathbf{R}_t = \mathbf{R}_{t-\Delta t} e^{i\sigma_c \Delta t} - i\sigma_c e^{-i\pi f_c \Delta t} \frac{(\mathbf{X}_t + \mathbf{X}_{t-\Delta t})}{2} \Delta t \tag{6}$$

where $\mathbf{R}_t$ and $\mathbf{X}_t$ indicate the discrete samples of $\mathbf{R}(t)$ and $\mathbf{X}(t)$ at time t, respectively, and $\mathbf{R}_0$ was set to be 0. Decomposed**C** contributions (**F** from **R**) is shown in Figures 1e and 1f.

2.2. Wavelet Transform Analysis

We used the MATLAB wavelet toolbox (Lilly, 2017) for frequency-time analysis of geophysical time series. The MATLAB function *cwt* provides the frequency-time spectrum of a time series based on a discretized version of the continuous wavelet transform, and the function *icwt* provides its inverse transform. The spectrum is provided with a set of complex numbers, and we used its magnitude to visualize frequency-time changes in figures below. The *cwt* and *icwt* functions use the generalized Morse wavelet with the symmetry parameter γ of 3 (perfectly symmetric) and the time-bandwidth product p^2 of 60 by default.

The inverse wavelet transform allows us to filter out chosen frequency-time windows to understand the timing of excitation changes that lead to CW amplitude reduction. We set the wavelet spectrum of **X** to 0 for the spectrum to be excluded, and 1 otherwise. Because the wavelet spectrum generally shows signals with gradual changes over frequency, such sharp rectangular window may lead to errors in the inverse transform and the estimated **C**. However, we find that the difference between the observed and reconstructed **C** is mostly due to the omitted spectrum of **X**, as will be discussed in the next section.

The inverse transforms of filtered spectra produce modified excitation functions, whose forced wobble contributions were computed via the discrete polar motion equation (Equation 6). Adding the free wobble component using the first value in 1980, we obtained estimates for **C** associated with frequency-time filtered excitation functions. The filtered (modified) excitation function is denoted as $\mathbf{X}'$, and similarly, the forced wobble and CW based on $\mathbf{X}'$ are indicated by $\mathbf{R}'$ and $\mathbf{C}'$, respectively. If the excluded spectrum is not important in the CW amplitude reduction event, then $\mathbf{C}'$ will be similar to **C** after 2015. Conversely, rejecting important frequency-time elements of the wavelet spectra will cause large differences between $\mathbf{C}'$ and **C** after 2015.

2.3. Other Estimates of Excitations

The Earth System Modeling GeoForschungsZentrum in Potsdam (ESMGFZ) (Dobslaw & Dill, 2018) provides Effective Angular Momentum (EAM) functions from 1976 to the present with the separate polar motion excitation contributions from angular momentum changes due to monthly mean mass distribution and motion of atmosphere (AAM), oceans (OAM), and terrestrial hydrosphere (HAM). Additionally, gravitational sea level change contributions derived from the mass change models are also provided separately (SLAM). The combined contribution of all EAM functions provides an estimate of the full excitation function Ψ. To obtain the contribution associated with **X** as in Equation 5, we reduced the ESMGFZ excitation functions by excluding linear and annual components, and then examined wavelet transform frequency-time spectra.

Satellite Laser Ranging (SLR) data (Cheng et al., 2011) provide an alternative observation of the mass change contributions to polar motion excitation. SLR data for low degree spherical harmonic (SH) Stokes coefficients are available since 2002, and the SH degree-2 and order-1 coefficients (denoted as C_{21} and S_{21}) can be converted into the x- and y-directional changes of the excitation function (Adhikari & Ivins, 2016; Chen et al., 2005; Youm et al., 2017), via

$$\begin{pmatrix}\psi_1\\ \psi_2\end{pmatrix} = -\sqrt{\frac{5}{3}}\,\frac{Ma^2}{(C-A)}\,\frac{1.098}{(1+k_2')}\begin{pmatrix}C_{21}\\ S_{21}\end{pmatrix} \tag{7}$$

where M and a represent the total mass and the mean radius of the Earth, respectively, and C and A are the polar and equatorial moment of inertia of the Earth, respectively. k_2' indicates the SH degree-2 load Love number. We used that contribution after removing annual and linear components as an alternative mass change contribution to **X**.

3. Results

3.1. Cancellation Between Free and Forced CW Components

Changes of **C** shown in Figures 1a and 1b can be decomposed into the free wobble (**F**) and forced wobble (**R**) contributions by using Equation 5 (Figures 1e and 1f). When the frequency signals of **X** create the forced wobble**R**, amplification is greatest near the CW frequency f_c (~0.8435 cpy) due to resonance, with varying amplification associated with the transfer function at other frequencies (Gross, 2000; Munk & MacDonald, 1960; Wilson, 1985; Wilson & Vicente, 1990). Thus the period of the forced wobble **R** is near 433 days on average, but appears irregular due to effects of the geophysical excitations which are amplified near f_c. The relative phase and amplitude differences between **F** and **R** effectively explain the observed **C** with irregularity of **R** being responsible for the large and rapid changes. For example, Figures 1e and 1f show phase differences between **F** and **R** over time. The amplitude of **C** was relatively large in the period 1990–1995 (Figures 1a and 1b), and changes of both **F** and **R** were in phase (Figures 1e and 1f). They are out of phase after ~2012, and have similar amplitudes as well after ~2015, leading to small amplitude of **C** for 2017–2021.

This explanation is consistent with the analogy of the free wobble as a slowly moving massive pendulum and the forced wobble being pendulum motion arising from small stones chaotically hitting it (Chao, 1985; Jeffreys, 1940). Using other P_c and Q_c values yields similar patterns (Figure S2 in Supporting Information S1). In particular, selecting an **F** that originated in the distant past (at t_0) and decays rapidly suggests that the CW amplitude reduction is entirely due to an amplitude decrease in **R** itself (e.g., Figures S2e and S2f in Supporting Information S1). In this case, excitation sources prior to t_0 are likely not responsible for the present-day **C**, as indicated by **F** ≈ 0. A condition where **R** ≈ 0 implies internal cancellation within **R** from t_0 to the present. To better interpret this, we introduce an intermediate reference time t_1 ($>t_0$), and re-define **F** from t_1. This new **F** includes the original **F** (from t_0) along with the accumulated **R** due to the earlier excitations from t_0 to t_1. The remaining **R**, arising from excitations from t_1 to the present, then effectively cancels this new **F** (from t_1), leading to the small amplitude of **C** after ~2015. In summary, the CW amplitude reduction is well reproduced by the cancellation between **F** and **R** regardless of the choice of initial time, and we selected $t_0 = 1980.0$ to demonstrate more evident cancellation effect between them.

3.2. Timing of Excitation Leading to CW Amplitude Reduction After 2015

Since **R** is due to geophysical excitation sources, we now examine **X** in more detail. The wavelet transform is useful to understand time-dependent changes of **X** at different frequencies. Figure 2 shows magnitude of the wavelet transform frequency-time spectrum of **X** from polar motion observations (without the annual frequency), which is dominated by periodicities shorter than a year for both positive and negative frequencies. For example, semi-annual changes were strong in 1985–1990, whereas intra-annual signals (between 1 and 2 cpy) show stronger amplitudes in 2000–2005 and 2010–2015. We also examined varied estimates of **X** based on a variety of P_c and Q_c values, finding that their frequency-time spectra were generally similar to one another (Figure S3 in Supporting Information S1).

Figure 3 shows the reconstruction of **C** (black curves in Figures 3b, 3d, 3f, and 3h) based on four different **X**′ (Figures 3a, 3c, 3e, and 3g), which are

Case 1 a wide positive frequency band from ~0.08 to ~5 cpy,
Case 2 a narrow frequency band around f_c: from 0.75 to 2 f_c (~0.6–~1.7 cpy),
Case 3 the narrow band without excitations in 2000 and 2001, and
Case 4 the narrow band without excitations in 2011 and 2012.

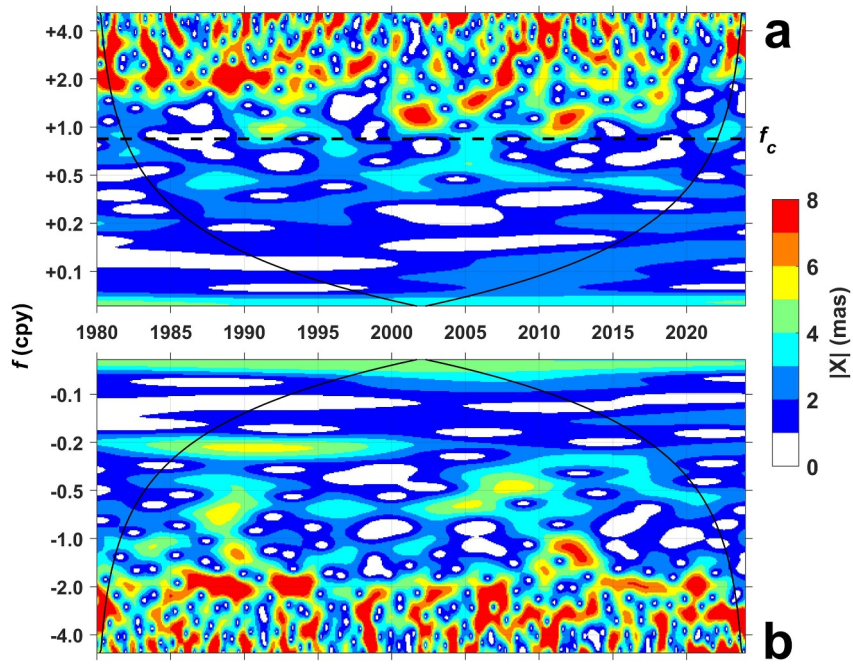

Figure 2. Magnitude of frequency-time spectrum of **X** from International Earth Rotation and Reference Service Earth Orientation Parameters C04 data via the wavelet transform. Positive and negative frequencies are displayed in panels (a, b), respectively. The dashed horizontal line indicates the Chandler Wobble frequency, f_c = 0.8435 cpy. The black solid curves represent the cone of influence, indicating that spectrum outside the cone has higher uncertainty.

These four **X**′ estimates were used to compute **C**′, to compare with **C** (observed). For example, **C**′ using a frequency band of **X** from ∼0.08 to ∼5 cpy (i.e., Case 1) was similar to the observed (Figure 3b). There are slight differences between **C**′ and **C** (red curve), which are mainly due to the omitted frequencies and numerical artifacts associated with discrete transforms (see Text S1 and Figure S1 in Supporting Information S1). An even narrower band from 0.75 to 2 f_c still yields a similar **C** (Case 2, Figures 3c and 3d). Using a band narrower than 0.75–2f_c resulted in a relatively large difference with observations, confirming the importance of this frequency band in the observed **C**.

We experimented with excluding signals near f_c for various time intervals to see how they affected CW amplitude reduction for 2017–2021. When excluding signals in the years 2000 and 2001 (Case 3, Figure 3e), the difference between **C** and **C**′ increases in amplitude after ∼2000. However, **C**′ still shows a somewhat reduced CW amplitude for 2017–2021 (Figure 3f), indicating that this period is not important in the CW amplitude reduction event. In contrast, we found that excitations in 2011 and 2012 are important in causing the CW amplitude reduction event (Case 4, Figures 3g and 3h). Removing the 2011–2012 excitations causes the amplitude of **R**′ to decrease by more than 50%, leading to incomplete signal cancellation between **F** and **R**′. As a result, the amplitude reduction event for 2017–2021 is virtually absent in **C**′ (Figure 3h). Similar behavior was found using various P_c and Q_c values (Figure S4 in Supporting Information S1).

Similar to Cases 3 and 4, we assessed excitation contributions for every year (see Figure S5 in Supporting Information S1), finding that excitations in 2002, 2005, and 2011–2012 were associated with the 2017–2021 CW amplitude reduction. However, the contribution from the period 2011–2012 was consistently the largest, regardless of P_c and Q_c choices.

3.3. Source of the Excitation Anomalies

The period 2011–2012 shows large intra-annual variability, but similar inter-annual variations appear at other times. Figure 4 compares frequency-time spectrum of geodetic **X** (Figure 4a) with a combinations of geophysical models and satellite observations since 2002 (Figures 4c and 4e), with Figure 4c being solely from ESMGFZ data (Dobslaw & Dill, 2018). Using the mass change estimates from SLR (Cheng et al., 2011) yields a similar

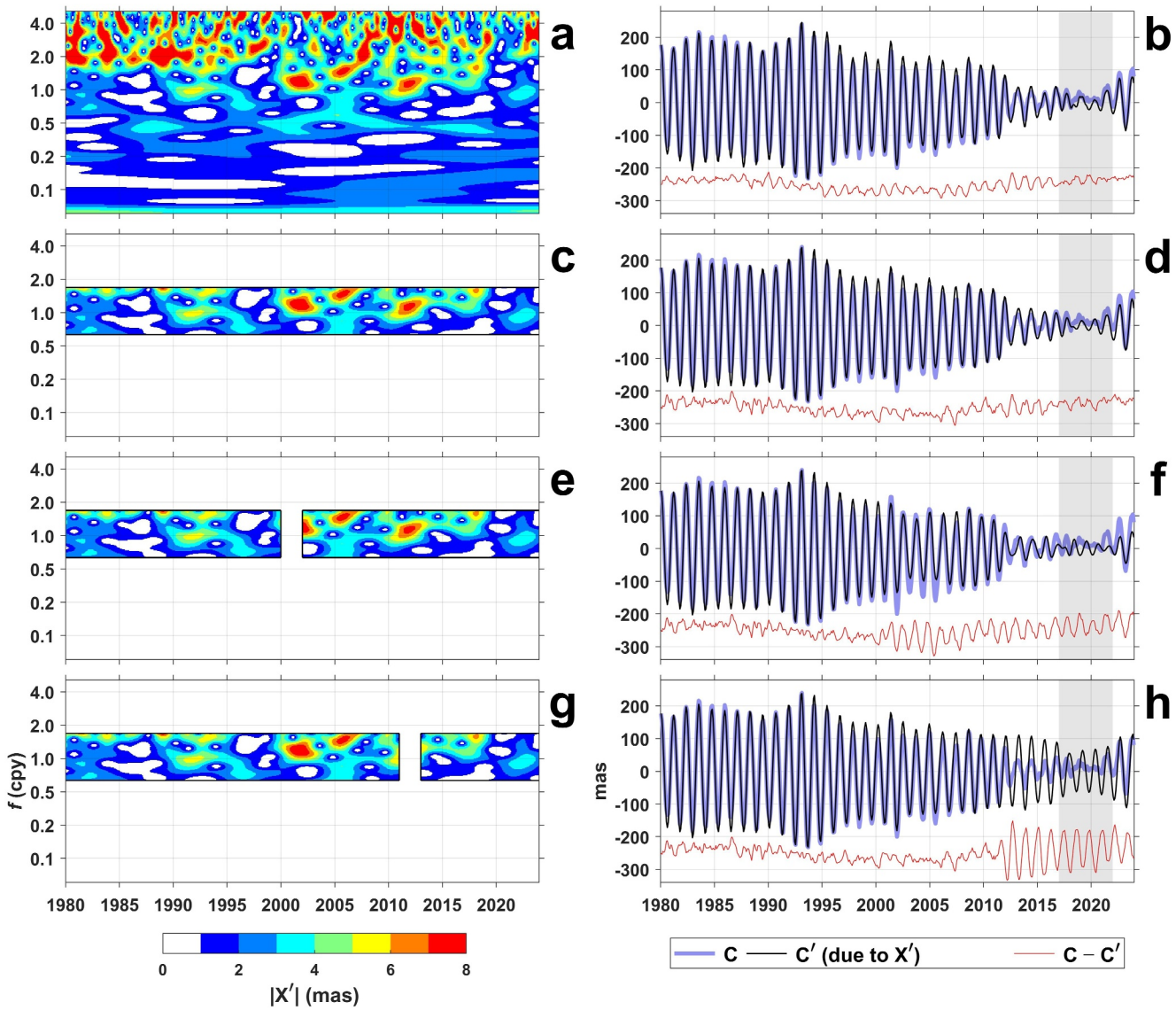

Figure 3. (a, c, e, and g) Four different $\mathbf{X}'$ from Cases 1, 2, 3, and 4 and (b, d, f, and h) reconstruction $\mathbf{C}'$. All $\mathbf{X}'$ are modified versions (via frequency-time filtering) of the geodetic $\mathbf{X}$. In the right panels, $\mathbf{C}'$ from $\mathbf{X}'$ were compared with $\mathbf{C}$ (observed, bright blue curve). The difference between $\mathbf{C}'$ and $\mathbf{C}$ are indicated by the red curves, offset by −250 mas for clarity. The *x*-component changes are shown here.

frequency-time pattern (Figure 4e), with both similar to the geodetic observations (Figure 4a). Relatively strong intra-annual anomalies appear in 2005 and 2011–2012, both associated with the CW amplitude reduction event in Figure S5 in Supporting Information S1. We examined the wavelet transform frequency-time spectra for individual contributions in ESMGFZ (Figure S6 in Supporting Information S1), finding that both terrestrial water storage and atmospheric mass and motion terms show relatively strong signals in a similar frequency band for 2011–2012. In particular, terrestrial water storage changes contribute significantly to the 2011 anomaly, with a smaller impact in 2005.

There was limited success in CW reconstruction using these estimates (Figures 4d and 4f). For example, the forced wobble using the sum of ESMGFZ products (red curve in Figure 4d) results in a large amplitude change of **C** since 2009 (black). This is largely due to signals near the annual frequency for 2006–2010 (mainly from mass terms in the model), which were not evident in geodetic **X** in Figure 4a. As shown in Figures 4g and 4h, excluding these spectra significantly improves the **R** and **C** estimates. Using SLR estimates as the mass term visibly suppresses the anomalies in 2006–2010 (Figure 4e), and results in **R** very close to the observed changes (red curve

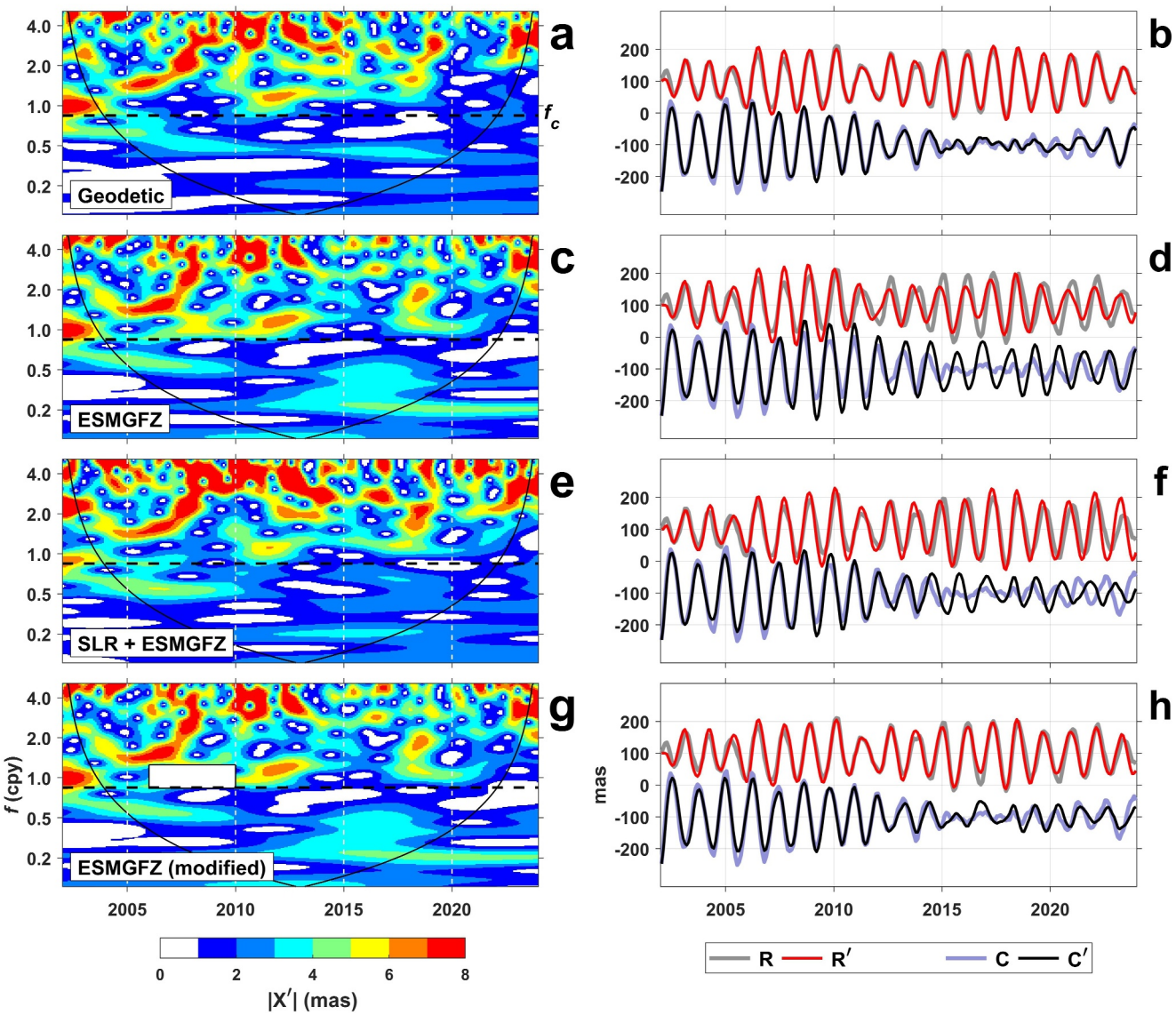

Figure 4. Frequency-time magnitude spectra of four different monthly $\mathbf{X}'$ from 2002.0 to 2024.0 (left column), and the corresponding $\mathbf{R}'$ and $\mathbf{C}'$ contributions (right column). For comparison, we included $\mathbf{C}$ and $\mathbf{R}$, obtained directly from polar motion data. (a) Similar to Figure 3a, but for a shorter period with available Satellite Laser Ranging (SLR) data. Since a shorter period was selected, the spectrum in the first couple of years (outside the cone of influence) has been slightly distorted compared to Figure 3a, due to the edge effect of wavelet analysis. (b) $\mathbf{C}'$ and $\mathbf{R}'$ based on the excitation spectrum in panel (a). (c, d) Similar to (a, b), respectively, but Earth System Modeling GeoForschungsZentrum in Potsdam products were used for the reconstruction. (e, f) Similar to (c, d), respectively, but the mass change contribution was replaced by the SLR estimate. (g, h) Similar to (c, d), but the spectrum within the open box (2006.0–2010.0) was excluded from the reconstruction. Here we used a wide frequency band from ∼0.15 to ∼5 cpy; as described in Figure 3, a narrower range of frequencies around f_c yields similar results. In panels (b, d, f, and h), varied offsets separate $\mathbf{R}$ (above) and $\mathbf{C}$ (below).

in Figure 4f). However, there are still phase differences, and the estimated $\mathbf{C}$ does not agree well with the observed. Using varied values for P_c and Q_c, it was also difficult to achieve good agreement in both amplitude and phase between predicted and observed (Figure S7 in Supporting Information S1).

4. Discussion and Conclusions

The recent CW amplitude reduction event can be interpreted as the cancellation between the free wobble and the forced wobble, which together have been in anti-phase since ∼2012. Our CW reconstruction tests provide clues about the timing of excitation sources resulting in a significant phase shift of the forced wobble. Considering both frequency-time magnitude changes of excitation functions and the frequency range creating a significant forced

wobble, the relatively strong intra-annual excitation variability, such as in 2011–2012, are likely the causes of the CW amplitude reduction. The variability is found in other geophysical model estimates and satellite observations. The models show the importance of atmosphere and terrestrial water storage changes in 2011–2012 intra-annual excitation variability.

Figure S5 in Supporting Information S1 shows that excitations in 2002, 2005, and 2011–2012 contributed significantly to CW amplitude reduction in 2017–2021. Years 2002, 2005, and 2011–2012 are also periods when the drift of the annual mean pole position shows a sharp orientation change, associated with the global wet and dry terrestrial water storage changes (Adhikari & Ivins, 2016). Boening et al. (2012) found that after a strong 2010–2011 La Niña event, continental-scale terrestrial water storage changes were followed by significant ocean mass loss due to changed precipitation and evaporation patterns, providing a possible cause of the CW reduction event.

CW amplitudes computed from model excitations do not account for the observed amplitude reduction after 2015 (Figure 4d). As tested in Figure 4h, small errors near the resonant frequency f_c can result in large differences in the computed CW. The excitation function is a globally integrated quantity, not tied to a single geographical region. This makes it challenging to identify possible error sources. However, as shown in frequency-time spectra in Figure 4 and Figure S7 in Supporting Information S1, contemporary geophysical models are approaching the quality needed to explain the observed CW.

Conflict of Interest

The authors declare no conflicts of interest relevant to this study.

Data Availability Statement

All data sets used in this study are publicly available. The EOP data from IERS is distributed from http://www.iers.org/IERS/EN/DataProducts/EarthOrientationData/eop.html. Products of the atmospheric, oceanic, and hydrological angular momentum by ESMGFZ are available from http://rz-vm115.gfz-potsdam.de:8080/repository. SLR-based degree-2 and order-1 Stokes coefficients are from Cheng et al. (2011). Additional data necessary to reproduce the results presented in this study are available from the Open Science Framework repository (Jeon, 2025).

Acknowledgments

We deeply appreciate the dedicated efforts of various research institutes for providing high-quality Earth rotation, excitation estimates, and other data freely available. We also gratefully acknowledge the constructive review comments from Dr. Masato Furuya, Dr. Ryuji Yamaguchi, and an anonymous reviewer, as well as the dedication of the editor, Dr. Monika Korte. This study was supported by the National Research Foundation of Korea (NRF) Grant (RS-2022-NR072315 and 2023R1A2C100489912) and the Korea Institute of Marine Science & Technology Promotion Grant funded by the Ministry of Oceans and Fisheries (RS-2023-00256677 [PM23030]). J.E. was supported by the NRF Grant (2021R1F1A1061854). JC was supported by the National Natural Science Foundation of China (42394132) and Hong Kong RGC Collaborative Research Fund (C5013-23G), and C.R.W. was supported by the NASA Earth Surface and Interior Program (80NSSC22K0906) and NASA GRACE Follow-On Science Program (80NSSC20K0820).

References

Adhikari, S., & Ivins, E. R. (2016). Climate-driven polar motion: 2003–2015. *Science Advances*, *2*(4), e1501693. https://doi.org/10.1126/sciadv.1501693

Bizouard, C., Lambert, S., Gattano, C., Becker, O., & Richard, J.-Y. (2019). The IERS EOP 14C04 solution for Earth orientation parameters consistent with ITRF 2014. *Journal of Geodesy*, *93*(5), 621–633. https://doi.org/10.1007/s00190-018-1186-3

Bizouard, C., Remus, F., Lambert, S. B., Seoane, L., & Gambis, D. (2011). The Earth's variable Chandler Wobble. *Astronomy and Astrophysics*, *526*, A106. https://doi.org/10.1051/0004-6361/201015894

Boening, C., Willis, J. K., Landerer, F. W., Nerem, R. S., & Fasullo, J. (2012). The 2011 La Niña: So strong, the oceans fell. *Geophysical Research Letters*, *39*(19), L19602. https://doi.org/10.1029/2012GL053055

Chao, B. F. (1985). On the excitation of the Earth' polar motion. *Geophysical Research Letters*, *12*(8), 526–529. https://doi.org/10.1029/GL012i008p00526

Chao, B. F., & Chung, W.-Y. (2012). Amplitude and phase variations of Earth's Chandler wobble under continual excitation. *Journal of Geodynamics*, *62*, 35–39. https://doi.org/10.1016/j.jog.2011.11.009

Chen, J. L., Wilson, C. R., & Tapley, B. D. (2005). Interannual variability of low-degree gravitational change, 1980–2002. *Journal of Geodesy*, *78*(9), 535–543. https://doi.org/10.1007/s00190-004-0417-y

Cheng, M., Ries, J. C., & Tapley, B. D. (2011). Variations of the Earth's figure axis from satellite laser ranging and GRACE. *Journal of Geophysical Research*, *116*(B1), B01409. https://doi.org/10.1029/2010JB000850

Ding, H., & Chao, B. F. (2017). Solid pole tide in global GPS and superconducting gravimeter observations: Signal retrieval and inference for mantle anelasticity. *Earth and Planetary Science Letters*, *459*, 244–251. https://doi.org/10.1016/j.epsl.2016.11.039

Dobslaw, H., & Dill, R. (2018). Predicting Earth orientation changes from global forecasts of atmosphere-hydrosphere dynamics. *Advances in Space Research*, *61*(4), 1047–1054. https://doi.org/10.1016/j.asr.2017.11.044

Fedorov, E. P., & Yatskiv, Y. S. (1965). The cause of the apparent "Bifurcation" of the free nutation period. *Soviet Astronomy*, *8*, 608–611.

Furuya, M., & Chao, B. F. (1996). Estimation of period and Q of the Chandler Wobble. *Geophysical Journal International*, *127*(3), 693–702. https://doi.org/10.1111/j.1365-246X.1996.tb04047.x

Gross, R. S. (2000). The excitation of the Chandler Wobble. *Geophysical Research Letters*, *27*(15), 2329–2332. https://doi.org/10.1029/2000GL011450

Gross, R. S. (2005). Oceanic excitation of polar motion: A review. In *Forcing of polar motion in the chandler frequency band: A contribution to understanding interannual climate change*. H. P. Plag, B. F. Chao, R. S. Gross, & T. van Dam (Eds.). (pp. 89–102). Centre Européen de Géodynamique et de Séismologie.

Guinot, B. (1972). The Chandlerian Wobble from 1900 to 1970. *Astronomy and Astrophysics*, *19*, 207.

Jeffreys, H. (1940). The variation of latitude. *Monthly Notices of the Royal Astronomical Society*, *100*(3), 139–155. https://doi.org/10.1093/mnras/100.3.139

Jeon, T. (2025). Diminished Chandler Wobble after 2015: Link to mass anomalies in 2011 [Dataset]. *OSF*. https://doi.org/10.17605/OSF.IO/YUBCV

Lilly, J. M. (2017). Element analysis: A wavelet-based method for analysing time-localized events in noisy time series. *Proceedings of the Royal Society A: Mathematical, Physical and Engineering Sciences*, *473*(2200), 20160776. https://doi.org/10.1098/rspa.2016.0776

Malkin, Z., & Miller, N. (2010). Chandler wobble: Two more large phase jumps revealed. *Earth Planets and Space*, *62*(12), 943–947. https://doi.org/10.5047/eps.2010.11.002

Munk, W. H., & MacDonald, G. J. F. (1960). *The rotation of the Earth: A geophysical discussion* (p. 323). Cambridge University Press.

Nastula, J., & Gross, R. (2015). Chandler Wobble parameters from SLR and GRACE. *Journal of Geophysical Research: Solid Earth*, *120*(6), 4474–4483. https://doi.org/10.1002/2014JB011825

Seitz, F., Kirschner, S., & Neubersch, D. (2012). Determination of the Earth's pole tide Love number k2 from observations of polar motion using an adaptive Kalman filter approach. *Journal of Geophysical Research*, *117*, B9. https://doi.org/10.1029/2012JB009296

Vondrak, J., & Ron, C. (2005). The great Chandler wobble change in 1923–1940 re-visited. *Cahiers du Centre Europeen de Geodynamique et de Seismologie*, *24*, 39–42.

Wilson, C. R. (1985). Discrete polar motion equations. *Geophysical Journal of the Royal Astronomical Society*, *80*(2), 551–554. https://doi.org/10.1111/j.1365-246X.1985.tb05109.x

Wilson, C. R., & Vicente, R. O. (1990). Maximum likelihood estimates of polar motion parameters. In *Variations in Earth rotation*. D. D. McCarthy & W. E. Carter (Eds.). (pp. 151–155). Americal Geophysical Union.

Xu, X.-Q., Fang, M., Zhou, Y.-H., & Liao, X.-H. (2024). Continental and oceanic AAM contributions to Chandler Wobble with the amplitude attenuation from 2012 to 2022. *Journal of Geodesy*, *98*, 6–59. https://doi.org/10.1007/s00190-024-01872-z

Yamaguchi, R., & Furuya, M. (2024). Can we explain the post-2015 absence of the Chandler Wobble? *Earth Planets and Space*, *76*(1), 1. https://doi.org/10.1186/s40623-023-01944-y

Youm, K., Seo, K.-W., Jeon, T., Na, S.-H., Chen, J., & Wilson, C. R. (2017). Ice and groundwater effects on long term polar motion (1979–2010). *Journal of Geodynamics*, *106*, 66–73. https://doi.org/10.1016/j.jog.2017.01.008